The Astrophysical Journal, 875:60 (9pp), 2019 April 10 https://doi.org/10.3847/1538-4357/ab0d90

The SAMI Galaxy Survey: Kinematic Alignments of Early-type Galaxies in A119 and A168

Hyunjin Jeong[1], Suk Kim[1], Matt S. Owers[2,3], Seok-Joo Joo[1,4,5], Hak-Sub Kim[1], Woong Lee[4], Youngdae Lee[1], Jesse van de Sande[6,7], Jaehyun Lee[8], Sukyoung K. Yi[9], Scott M. Croom[6,7], Julia J. Bryant[6,7,10], Soo-Chang Rey[4], Sarah Brough[7,11], Sree Oh[7,12], Nicholas Scott[6,7], Chiara Tonini[13], Anne M. Medling[12,14,19], Sarah M. Sweet[7,15], Joss Bland-Hawthorn[6], Iraklis S. Konstantopoulos[16], J. S. Lawrence[17], and Samuel N. Richards[18]
[1] Korea Astronomy & Space Science institute, 776, Daedeokdae-ro, Yuseong-gu, Daejeon 34055, Republic of Korea; hyunjin@kasi.re.kr
[2] Department of Physics and Astronomy, Macquarie University, NSW 2109, Australia
[3] Astronomy, Astrophysics and Astrophotonics Research Centre, Macquarie University, Sydney, NSW 2109, Australia
[4] Department of Astronomy and Space Science, Chungnam National University, 99 Daehak-ro, Daejeon 34134, Republic of Korea
[5] Research Institute of Natural Sciences, Chungnam National University, 99 Daehak-ro, Daejeon 34134, Republic of Korea
[6] Sydney Institute for Astronomy, School of Physics, A28, The University of Sydney, NSW 2006, Australia
[7] ARC Centre of Excellence for All Sky Astrophysics in 3 Dimensions (ASTRO 3D)
[8] Korea Institute for Advanced Study, 85, Hoegi-ro, Dongdaemun-gu, Seoul 02455, Republic of Korea
[9] Department of Astronomy and Yonsei University Observatory, Yonsei University, Seoul 03722, Republic of Korea
[10] Australian Astronomical Optics, AAO-USydney, School of Physics, University of Sydney, NSW 2006, Australia
[11] School of Physics, University of New South Wales, NSW 2052, Australia
[12] Research School of Astronomy and Astrophysics, The Australian National University, Canberra, ACT 2611, Australia
[13] School of Physics, Melbourne University, Parkville, VIC 3010, Australia
[14] Ritter Astrophysical Research Center University of Toledo Toledo, OH 43606, USA
[15] Centre for Astrophysics and Supercomputing, Swinburne University of Technology, P.O. Box 218, Hawthorn, VIC 3122, Australia
[16] Atlassian 341 George St Sydney, NSW 2000, Australia
[17] Australian Astronomical Optics—Macquarie, Macquarie University, NSW 2109, Australia
[18] SOFIA Science Center, USRA, NASA Ames Research Center, Building N232, M/S 232-12, P.O. Box 1, Moffett Field, CA 94035-0001, USA
Received 2018 December 11; revised 2019 February 25; accepted 2019 March 2; published 2019 April 16

Abstract

We investigate the kinematic alignments of luminous early-type galaxies ($M_r \leqslant -19.5$ mag) in A119 and A168 using the kinematic position angles (PA_{kin}) from the Sydney-AAO Multi-object Integral-field spectrograph (SAMI) survey data, motivated by the implication of the galaxy spin alignment in a cosmological context. To increase the size of our sample for statistical significance, we also use the photometric position angles (PA_{phot}) for galaxies that have not been observed by SAMI, if their ellipticities are higher than 0.15. Our luminous early-type galaxies tend to prefer the specific position angles in both clusters, confirming the results of Kim et al., who recently found the kinematic alignment of early-type galaxies in the Virgo cluster based on the ATLAS^{3D} integral-field spectroscopic data. This alignment signal is more prominent for galaxies in the projected phase-space regions dominated by infalling populations. Furthermore, the alignment angles are closely related to the directions of the filamentary structures around clusters. The results lead us to conclude that many cluster early-type galaxies are likely to be accreted along filaments while maintaining their spin axes, which are predetermined before cluster infall.

Key words: galaxies: clusters: individual (A119 and A168) – galaxies: evolution – galaxies: formation – galaxies: kinematics and dynamics

Supporting material: machine-readable table

1. Introduction

Galaxies are predicted to have spin vectors aligned with nearby large-scale structures, according to the tidal torque theory (Hoyle 1949; Peebles 1969; White 1984). If the primordial angular momentum is conserved, galaxy spin vectors at the present epoch still correlate with the large-scale structures. However, in the Λ cold dark matter (ΛCDM) paradigm, galaxies are expected to grow through numerous mergers, which may have a significant influence on their angular momentum. Hence, studying the alignment between galaxy spin axes and large-scale structures can provide vital information about how galaxies form and evolve.

Several attempts have been made to test the alignment of galaxy spin vectors in simulations (see, e.g., Navarro et al. 2004; Aragón-Calvo et al. 2007; Brunino et al. 2007; Paz et al. 2008; Hahn et al. 2010; Codis et al. 2012; Dubois et al. 2014; Wang & Kang 2018). For instance, Aragón-Calvo et al. (2007) showed that a correlation between galaxy spin vectors and large-scale structures depends on halo mass. Codis et al. (2012) also claimed that low-mass halos acquire a spin parallel to the direction of the host filament, while more massive halos acquire a spin perpendicular to the host filament direction, because of mergers along the filaments. More recently, using the hydrodynamical cosmological volume simulation, Horizon-AGN, Dubois et al. (2014) found that the stellar mass transition from alignment to misalignment (or perpendicular alignment) happens around $3 \times 10^{10} M_{\odot}$, in quantitative agreement with the transition mass of Codis et al. (2012) for dark matter.

Observational attempts have also been made to test these theoretical predictions (see, e.g., Lee 2004; Trujillo et al. 2006; Paz et al. 2008; Tempel & Libeskind 2013; Tempel et al. 2013; Pahwa et al. 2016). For example, using the Sloan Digital Sky Survey (SDSS; York et al. 2000) data, Tempel et al. (2013)

[19] Hubble Fellow.

found that the spin axes of bright spiral galaxies tend to be weakly aligned parallel to their host filaments, while the spin axes of early-type galaxies have a strong tendency to be aligned perpendicular to the host filaments. This was confirmed by Pahwa et al. (2016) based on the 2 Micron All-Sky Survey (Huchra et al. 2012) data.

In cluster environments, the densest regions in the universe found at the nodes of filamentary structures, galaxy spin axes are a priori expected to be distributed either randomly or anisotropically. Indeed, Aryal & Saurer (2004, 2005) showed that the photometric position angle (PA_{phot}) distribution of galaxies in Abell clusters varies from cluster to cluster, that is, galaxies in some clusters are well aligned, while others have no preferred spin axes. Recently, Kim et al. (2018) found a clear alignment for the Virgo early-type galaxies using stellar kinematic position angles (PA_{kin}) from ATLAS^{3D}. Moreover, according to Lee et al. (2018), who performed an analysis on the YZiCS cluster simulations (Choi & Yi 2017), a galaxy spin axis acquired within a large-scale structure can be preserved for many gigayears, even after entering a cluster.

Focusing on early-type galaxies is well suited for investigating the kinematic alignment of cluster galaxies, because early-type galaxies are believed to form as a result of mergers that make a galaxy spin axis perpendicular to the host filament. Furthermore, the PA_{kin} values, defined as the angle between the north and the receding part of the velocity map in a counterclockwise direction (i.e., perpendicular to the spin axis), is the best indicator to determine the galaxy spin axis, particularly for a round galaxy, for which it is difficult to estimate its major axis (hence its spin axis) based on photometric data. Therefore, PA_{kin}-extracted from integral-field spectroscopic (IFS) observations can provide a better understanding of the correlation between the spin axes of early-type galaxies and filamentary structures. The Sydney-AAO Multi-object Integral-field spectrograph (SAMI; Croom et al. 2012), mounted on the 3.9 m Anglo-Australian Telescope (AAT) and fed into the AAOmega dual-beamed spectrograph (Sharp et al. 2006), with 13 fused fiber bundles (Hexabundles; Bland-Hawthorn et al. 2011; Bryant et al. 2014) of $\sim 15''$ diameter on the sky, makes it possible to obtain spatially resolved optical spectra for a large number of galaxies.

The SAMI Galaxy Survey provides a complete census of the resolved optical properties (e.g., star formation rate, age, metallicities, and stellar and ionized gas kinematics) of ~3000 galaxies in the redshift range $0.004 < z < 0.095$ (Bryant et al. 2015) from the Galaxy And Mass Assembly survey (GAMA; Driver et al. 2011) and in eight clusters (APMCC0917, A168, A4038, EDCC442, A3880, A2399, A119, and A85 at $0.029 < z < 0.058$; Owers et al. 2017). The public data[20] are accessible via the survey website[21] (Allen et al. 2015; Green et al. 2018; Scott et al. 2018), and the Australian Astronomical Observatory's Data Central.[22]

In this study, we focus on early-type galaxies in A119 and A168 that are directly linked to a filament with similar redshifts (see Table 1 and Figure 12). Our sample is described in Section 2, and the properties of our sample galaxies in A119 and A168 are presented in Sections 3 and 4, respectively. Subsequently, in Section 5, we discuss the connection between the kinematic alignment of cluster early-type galaxies and their surrounding filamentary structures, before conclusions are drawn. Throughout the paper, we adopt a standard ΛCDM cosmology with $\Omega_m = 0.3$, $\Omega_\Lambda = 0.7$, and $H_0 = 70\,\mathrm{km\,s^{-1}\,Mpc^{-1}}$.

[20] Note that the cluster data are not yet included in the public data set.
[21] https://sami-survey.org/data/
[22] http://www.asvo.org.au/index.php/aao-data-central/

Table 1
The Properties of A119 and A168

Cluster	R.A. J2000	Decl. J2000	z	M_{200} ($10^{14}M_\odot$)	R_{200} (Mpc)
A119	14.067150	−1.255370	0.0442	8.6 ± 3.1	2.04
A168	18.815777	0.213486	0.0449	1.9 ± 1.1	1.32

Note. R.A., decl., z, M_{200}, and R_{200} are all from Owers et al. (2017).

2. Data and Sample

We begin by selecting all member galaxies in A119 and A168 from Owers et al. (2017) observed as part of the SAMI survey. Note that the SAMI redshift catalog for cluster galaxies has a high spectroscopic completeness (~85% for A119 and ~95% for A168) for $r_{petro} \leqslant 19.4$ and cluster-centric distances $R < 2R_{200}$. The morphological classification to select early-type galaxies is based on visual inspection by five authors using both the SDSS DR14[23] and the Dark Energy Camera Legacy Survey[24] color-composite images. Our classifications are carried out using a scheme of two classes: early-type and others. The results are collated, and galaxies with at least 80% of the vote are classified as early-types to construct a robust sample.

The absolute r-band magnitude cut of −19.5 mag,[25] taking the optical magnitudes from Owers et al. (2017), is applied on a sample in order to exclude dwarf-scale galaxies, because the alignment between galaxy spin axes and filaments is known to be correlated with galaxy luminosity (Tempel et al. 2013; Pahwa et al. 2016).

To investigate the kinematic alignment of cluster early-type galaxies, we use the values of PA_{kin} from SAMI. The SAMI stellar kinematic maps are obtained using the Penalized Pixel-Fitting (Cappellari & Emsellem 2004) routine as described in van de Sande et al. (2017), and the values of PA_{kin} are derived from the stellar kinematic maps using the Fit Kinematic PA code that is based on the method described in Appendix C of Kranović et al. (2006; see Section 6.1.6 of Scott et al. 2018). The standard SAMI data reduction method is described in Sharp et al. (2015).

Among our sample, only about 60% of galaxies have the values of PA_{kin}.[26] However, it is known that a small fraction of early-type galaxies (~10% from Kranović et al. 2011 based on ATLAS^{3D} and ~27% from Fogarty et al. 2015 using the SAMI pilot data) exhibit a significant difference between PA_{phot} and PA_{kin}. In Figure 1, we show the kinematic misalignment angle (Ψ, which is defined as $\sin\Psi = |\sin(PA_{phot} - PA_{kin})|$) of luminous early-type galaxies ($M_r \leqslant -19.5$ mag) in A119

[23] https://www.sdss.org/dr14/
[24] legacysurvey.org/decamls/
[25] For a sanity check, we apply the various r-band magnitude cuts of −21.0, −20.5, −20.0, and −19.0 on our sample, and note that the results are not affected by the selection of the magnitude cut, except for the significance level. Furthermore, if a galaxy is fainter than −19.0 in r-band ($\sim 10^{10}\,M_\odot$, when we assume that $g-r = 0.8$), it begins to become difficult to measure kinematics for passive systems.
[26] The SAMI survey included galaxies within $R < R_{200}$ as primary targets, so the majority of the galaxies without PA_{kin} are likely to be outside that radius.

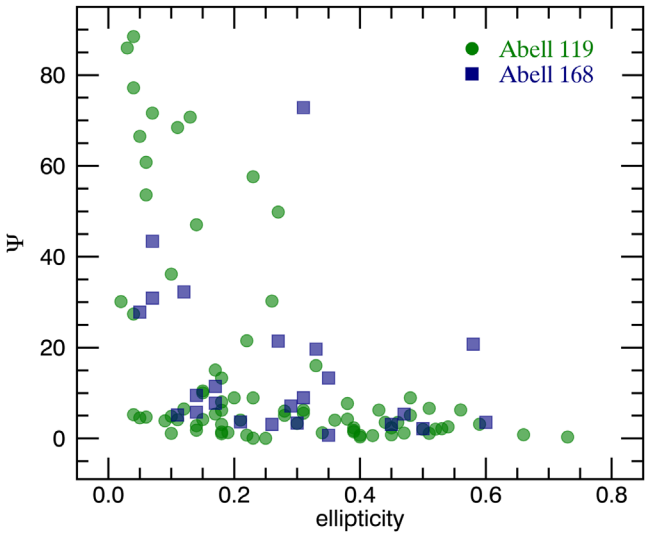

Figure 1. Kinematic misalignment angle Ψ, defined as the difference between the photometric position angle (PA_{phot}) and the kinematic position angle (PA_{kin}), as a function of ellipticity for luminous early-type galaxies ($M_r \leqslant -19.5$ mag) in A119 (green circles) and A168 (blue squares).

(green circles) and A168 (blue squares) as a function of ellipticity, by measuring the values of PA_{phot} and ellipticity using SExtractor (Bertin & Arnouts 1996). The agreement between PA_{phot} and PA_{kin} is generally good, but some galaxies with small ellipticities ($\epsilon < 0.15$, that is, round galaxies) show a clear discrepancy. When we adopt the ATLAS^{3D} constraint, $\Psi < 15°$ (Kranović et al. 2011), 74% of our sample galaxies are in this range, and if we select galaxies with larger ellipticity ($\epsilon \geqslant 0.15$), the fraction increases to 87%. This also means that 13% of our sample galaxies with large ellipticities show differences in PA_{phot} and PA_{kin} values. A difference between these two PAs can be indicative of the intrinsic shape of a galaxy (triaxiality) or caused by strong bars or galaxy interactions. In particular, galaxies with large kinematic misalignment angles ($\Psi > 20°$) and ellipticities ($\epsilon > 0.20$) are likely to be dominated by strong bars or interacting systems, according to Weijmans et al. (2014) based on the ATLAS^{3D} data and Oh et al. (2016) using the SAMI and CTIO deep imaging data. Indeed, seven galaxies with large Ψ and ϵ in our sample tend to have disturbed features.

To increase the sample size, we use PA_{phot} for galaxies that have not been observed by SAMI, if its ellipticity is larger than 0.15.[27] We also rearrange the values of PA_{kin} to lie between 0° and 180° by considering neither the receding nor the preceding parts of the velocity map, in accordance with the range of PA_{phot}. These processes yield a final sample of 133 and 40 galaxies for A119 and A168, respectively, and the details are listed in Table 2.

3. Properties of Early-type Galaxies in A119

A119 ($z \sim 0.0442$) is a relatively rich cluster among SAMI cluster samples, with $M_{200} \sim 8.6 \times 10^{14}\, M_{\odot}$ and $R_{200} \sim 2.04$ Mpc (Owers et al. 2017). This cluster exhibits a prominent red sequence dominated by early-type galaxies, as presented in Figure 2, and the brightest cluster galaxy (BCG) is located in the cluster center, as if it is a virialized system.

[27] For reference, 17 and 6 galaxies are excluded in A119 and A168, respectively, and we note that our results are not changed by including them.

Table 2
Results of Sample Selection

Cluster	N_{mem}	N_{ETG}	$N_{ETG,PA_{kin}}$
A119	695	133	79
A168	364	40	24

Note. N_{mem} is the total number of member galaxies in each cluster from Owers et al. (2017). N_{ETG} is the total number of luminous early-type members ($M_r \leqslant -19.5$ mag) that are used in this study, while $N_{ETG,PA_{kin}}$ is the number of galaxies with the PA_{kin} from SAMI among our sample.

Previous studies, however, suggest that A119 is a dynamically young cluster with several substructures (see, e.g., Fabricant et al. 1993; Rossetti & Molendi 2010; Lee et al. 2016), and the galaxy density map is elongated in the northeast direction (Owers et al. 2017).

3.1. Distribution of Early-type Galaxies in A119

The spatial distribution of our 133 luminous early-type sample galaxies in A119 is illustrated in Figure 3 as green ellipses, based on their PA_{phot} or PA_{kin} and ellipticities, together with cluster member galaxies (gray circles). The BCG lives in the densest part of A119, the rough center of the cluster and the main concentration of X-ray emission (red cross), and early-type galaxies are relatively evenly distributed within $0.6R_{200}$ by reference to R_{200}, denoted by the black dashed circle. To the northeast of the BCG, however, there exists an over-density region containing many early-type galaxies (see the number density contours of cluster member galaxies (black) and green ellipses), as already known (see, e.g., Lee et al. 2016; Owers et al. 2017). This anisotropic galaxy distribution in a cluster is common in the ΛCDM cosmology in which galaxy clusters are hierarchically assembled with structure formation.

3.2. Alignment Signal in A119

The position angle (PA) distribution (top) and the probability distribution function (PDF; bottom) of $1+\xi$ (where ξ is the excess probability)[28] for our sample galaxies are shown in Figure 4. Our luminous early-type sample galaxies prefer the specific PA value of $\sim 95°$ (hereafter, the kinematic alignment angle). This implies that the findings of Kim et al. (2018) are not limited to the Virgo cluster.

We also perform 1000 bootstrap resampling for PA values of A119 with the same number of sample galaxies (#133 for A119) to estimate the uncertainty of the kinematic alignment angle measurement. As a result, the mean and standard deviation of 1000 PA peak values are 90° and 25°, respectively.

To test the statistical significance of our finding, we use bootstrap resampling methods again. After 1000 iterations, the uniform distribution is generated and the 1σ confidence level is calculated (gray solid line and gray shaded regions in the bottom panel of Figure 4). The values of PDF for our sample and the uniform distribution at $PA \sim 95°$ are 1.62 and 1.00, respectively, and the 1σ level is 0.20. This means that the

[28] An excess probability distribution shows the probability that a measure will take any value greater than a particular number. For example, if a particular number of a bin is A and the measured value of that bin is also A, then $1+\xi$ is $1(=A \div A)$. In other words, if the number of samples in each bin is the same (i.e., uniform distribution), then $1+\xi$ is 1 in all ranges.

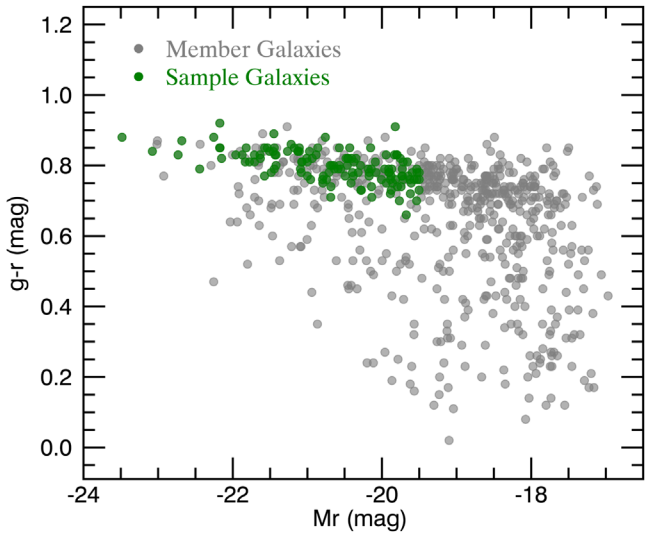

Figure 2. Color–magnitude relation of A119. Our sample galaxies (i.e., luminous early-type galaxies) are presented as green circles with cluster member galaxies as gray circles.

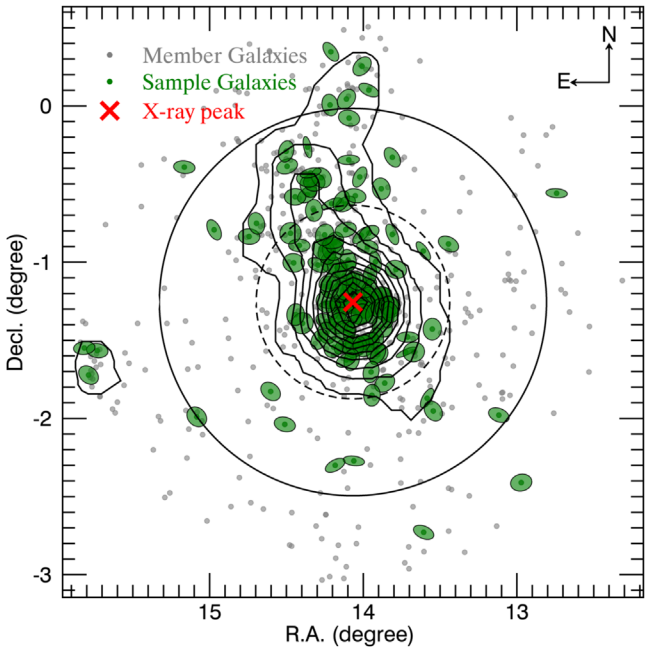

Figure 3. Spatial distribution of member galaxies in A119. The green ellipses indicate our 133 luminous early-type sample galaxies, while the gray circles are member galaxies in A119. For the ellipse, the length of the major axis is given a fixed value, but the orientation of the major axis and the length of the minor axis reflect the values of PA_{phot} or PA_{kin}, and the ellipticity of each galaxy. The black contours represent the galaxy number density, whereas the black dashed and solid circles indicate R_{200} and $2R_{200}$, respectively. The red cross marks the peak of X-ray emission from the *ROSAT* observations.

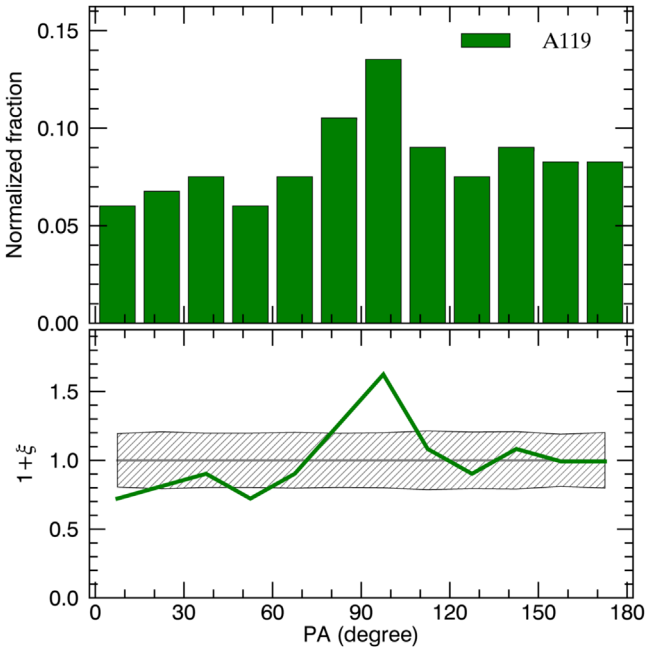

Figure 4. Distribution of the position angles (PA; top) and the probability distribution function (PDF; bottom) of $1+\xi$ for our 133 luminous early-type sample galaxies in A119, with a bin width of 15°. The PDF of the uniform distribution is shown as the gray solid line in the bottom panel, and the 1σ confidence level is also presented as gray shaded regions.

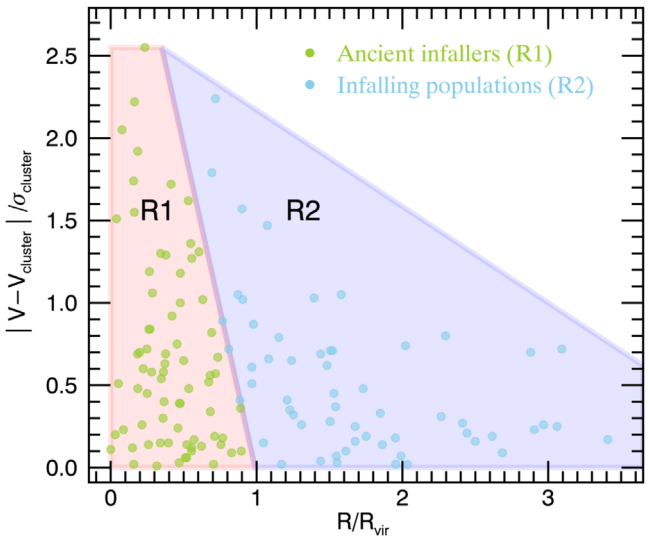

Figure 5. Phase-space diagram for our 133 luminous early-type sample galaxies in A119, split up into two distinct regions (labeled R1 and R2). The sample galaxies are divided into two subsamples based on the position in a phase-space diagram, following the classification introduced by Rhee et al. (2017): R1 corresponds to regions B, C, and E in their Figure 6, and R2 to regions A and D. Light green indicates ancient infallers (73 galaxies), while sky blue denotes infalling populations (60 galaxies). R_{vir} is calculated by dividing 0.8 by R_{200}.

alignment signal in A119 is significant at the 3σ confidence level.

According to Lee et al. (2018), cluster environments do not efficiently re-orient galaxy spin vectors unless a merger or strong tidal perturbation was encountered. Nevertheless, the change in the spin axis tends to increase with time after infall of a galaxy into the cluster, regardless of mergers (see panel (d) of Figure 5 of Lee et al. 2018). We, therefore, divide the sample into two subsamples based on the distribution of the population for a particular time since infall, in a projected phase-space diagram from Rhee et al. (2017, Figure 6), as shown in Figure 5: (1) galaxies in R1 (light green circles, 73 galaxies found in the projected phase-space region that is dominated by ancient infallers) and (2) galaxies in R2 (sky blue circles, 60 galaxies in the region dominated by infalling populations). Rhee et al. (2017) performed phase-space analyses in cluster environments using the YZiCs data (Choi & Yi 2017) and found that galaxies tend to follow a certain path in a phase-

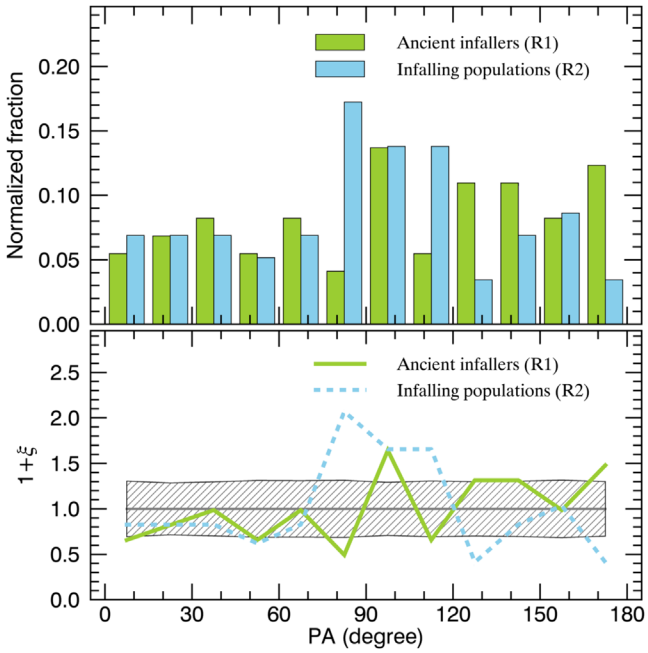

Figure 6. Same as Figure 4, but for two subsamples divided by the position in a phase-space diagram (see Figure 5). Light green indicates ancient infallers (73 galaxies in R1 of Figure 5), while sky blue represents infalling populations (60 galaxies in R2 of Figure 5). The PDF of the uniform distribution is also shown for comparison in gray, with the 1σ confidence level in the bottom panel.

space diagram based on the time since infall into a cluster.[29] They divided the phase space into five distinct regions, but we divide our sample galaxies into two subsamples for statistical significance.

Figure 6 presents the PA distributions and PDFs of $1+\xi$ for our subsamples. Galaxies in the outer regions of the cluster (R2 in Figure 5, sky blue histograms and the dashed line PDF) exhibit a more prominent alignment signal (almost 3.5σ level), even though the kinematic alignment angle is a little shifted toward 80°, compared with the parent sample (see Figure 4). As an additional step, to quantify the statistical significance of the alignment signal for galaxies in the outer parts of the cluster, we perform the Kuiper and Watson tests for the PDFs of A119 and the uniform distribution. Both tests give a probability of <0.01, so the null hypothesis of no difference is rejected. On the other hand, the alignment signal for galaxies closer to the cluster center (R1 in Figure 5, light green histograms and the solid line PDF) does not disappear completely, but it is considerably weakened, as can be expected from the results of Lee et al. (2018).

4. Properties of Early-type Galaxies in A168

A168 ($z\sim0.0449$) is well known as a cluster–cluster merger, with $M_{200}\sim1.9\times10^{14}\,M_{\odot}$ and $R_{200}\sim1.32$ Mpc (Owers et al. 2017). From the *Chandra* observations, this cluster has two peaks of X-ray emission in the central parts and the northern parts of the cluster (Hallman & Markevitch 2004; Fogarty et al. 2014, see also the red crosses in Figure 8). The strongest X-ray emission peak is the northern one corresponding to the BCG of this cluster, but the galaxy number density peak is not coincident with either of the X-ray peaks. The color–magnitude relation of this cluster, presented in Figure 7, is also unusual: (1) the BCG is at least 1 mag brighter than the second brightest galaxy and (2) the red sequence is not prominent in comparison with other clusters, such as A119 (see Figure 2).

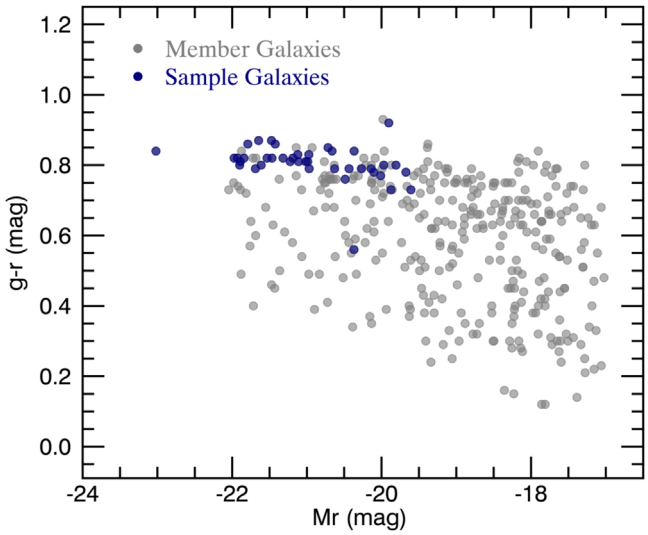

Figure 7. Color–magnitude relation of A168. Our sample galaxies (i.e., luminous early-type galaxies) are denoted as blue circles together with cluster member galaxies as gray circles.

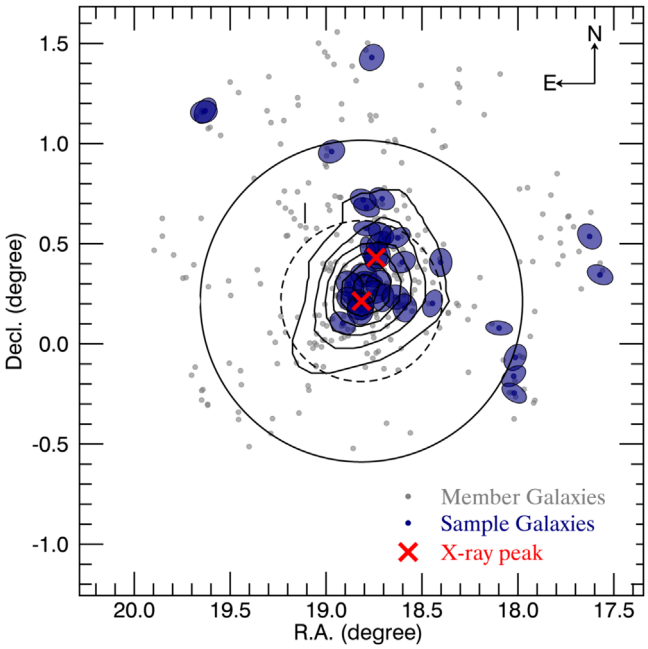

Figure 8. Spatial distribution of member galaxies in A168. The blue ellipses indicate our 40 luminous early-type sample galaxies, while the gray circles are member galaxies in A168. Symbols are the same as in Figure 3, except that two X-ray peaks come from the *Chandra* observations.

4.1. Distribution of Early-type Galaxies in A168

The spatial distribution of our 40 luminous early-type galaxies in A168 is shown in Figure 8 as blue ellipses with cluster member galaxies (gray circles). Early-type galaxies in this cluster are mainly situated around the two X-ray peaks, and the fraction of luminous early-type galaxies is low compared with that of A119, 13% correspond to 22%. Many observational studies suggest that a cluster merger is likely to trigger

[29] For reference, Noble et al. (2013) also tried to separate cluster members into "accreted early" and "accreted recently" galaxies, utilizing caustic diagrams.

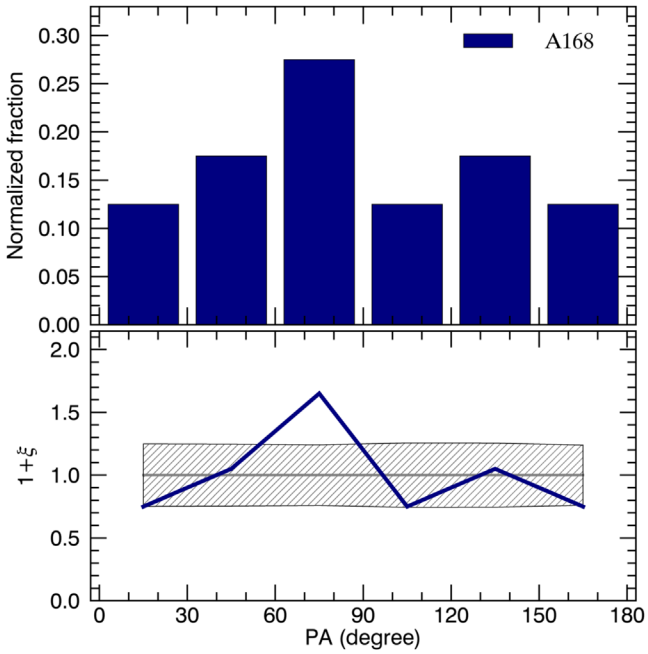

Figure 9. The PA distribution (top) and the PDF of $1+\xi$ (bottom) for our 40 luminous early-type sample galaxies in A168, with a bin width of 30°. For comparison, the PDF of the uniform distribution with the 1σ confidence level is shown in gray in the bottom panel.

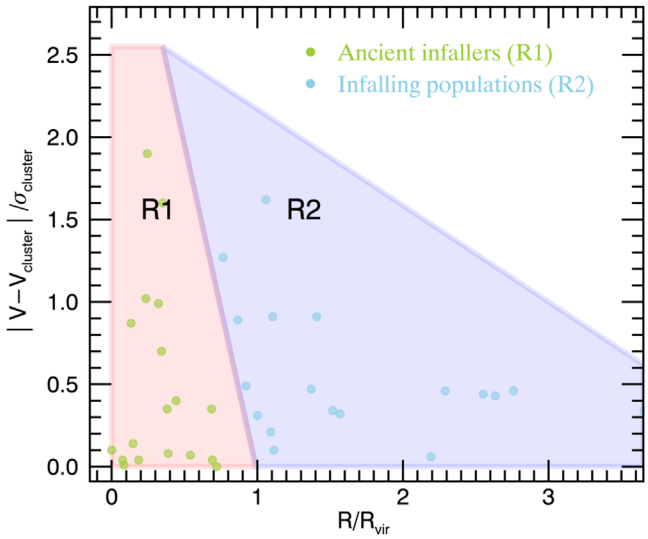

Figure 10. Phase-space diagram for our 40 luminous early-type sample galaxies in A168, split up into two regions (see Figure 5 and Section 3.2). Light green represents ancient infallers (18 galaxies), while sky blue indicates infalling populations (22 galaxies).

star formation activity of cluster galaxies depending on the merging stage (see, e.g., Caldwell et al. 1993; Caldwell & Rose 1997; Ferrari et al. 2005; Hwang & Lee 2009). It is unclear whether the properties of our sample galaxies have been impacted during a cluster–cluster merger, but if star formation activity is enhanced by this process, it may also affect the kinematics of our sample galaxies.

4.2. Alignment Signal in A168

We present the PA distribution (top) and the PDF (bottom) of $1+\xi$ for our sample galaxies in Figure 9 and find that early-type galaxies in A168 tend to prefer a specific PA value of

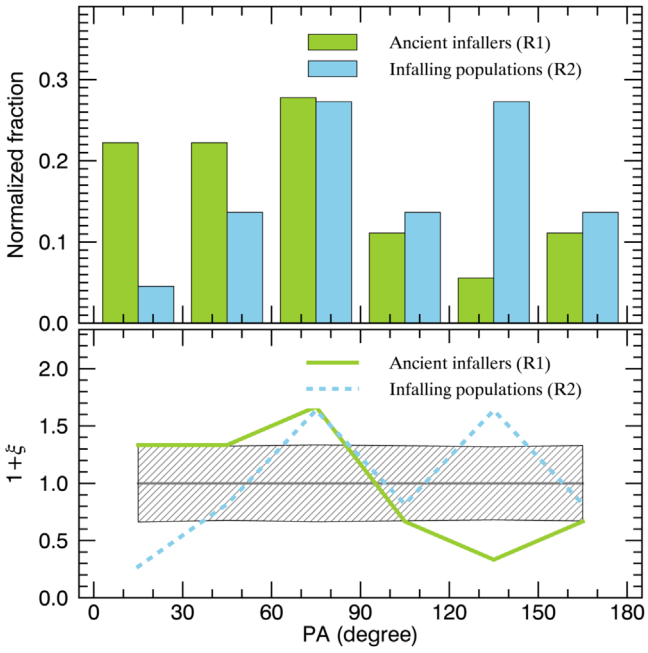

Figure 11. Same as Figure 9, but for two subsamples divided by the position in a phase-space diagram (see Figure 10). Light green represents ancient infallers (18 galaxies in R1 of Figure 10), while sky blue indicates infalling populations (22 galaxies in R2 of Figure 10). The PDF of the uniform distribution is also shown for comparison in gray, with the 1σ confidence level in the bottom panel.

roughly 75°. This implies that early-type galaxies could be kinematically aligned with each other in terms of PA, even in merging clusters, although the peak of the PA distribution for A168 is at the 2.7σ confidence level. We also estimate the mean and standard deviation of the kinematic alignment angle of A168 (see Section 3.2 for methodology), and the values are 72° and 25°, respectively. As compared to A119, the weakened alignment signal might be related to the nature of this cluster (i.e., cluster–cluster merging) and/or the filamentary structures of this cluster.

The phase space of A168 divided into two regions is shown in Figure 10, as we have tested the A119 galaxies (see Figure 5 and Section 3.2): (1) ancient infallers (18 galaxies in R1, light green circles) and (2) infalling populations (22 galaxies in R2, sky blue circles).

In Figure 11, we present the PA distributions and PDFs of $1+\xi$ for our subsamples. Light green histograms and the solid line PDF indicate 18 ancient infallers, and sky blue histograms and the dash line PDF represent 22 infalling populations. Although the statistical significance is low as $\sim 2.0\sigma$ level because our analysis for A168 is based on a limited sample, the kinematic alignment angle of A168 corresponds to those of subsamples. In addition, for infalling populations (galaxies in R2 of Figure 10), another peak of the PA distribution at roughly 135° is revealed. However, it is necessary to keep in mind that A168 is known as a cluster–cluster merger with two X-ray peaks, so the cluster center position may be inaccurate.

5. Discussion and Conclusions

Galaxy clusters are the most massive virialized objects in the universe. They are usually connected to multiple filaments that arrive from various directions at the same time, so the kinematic alignment angles of cluster galaxies can be found

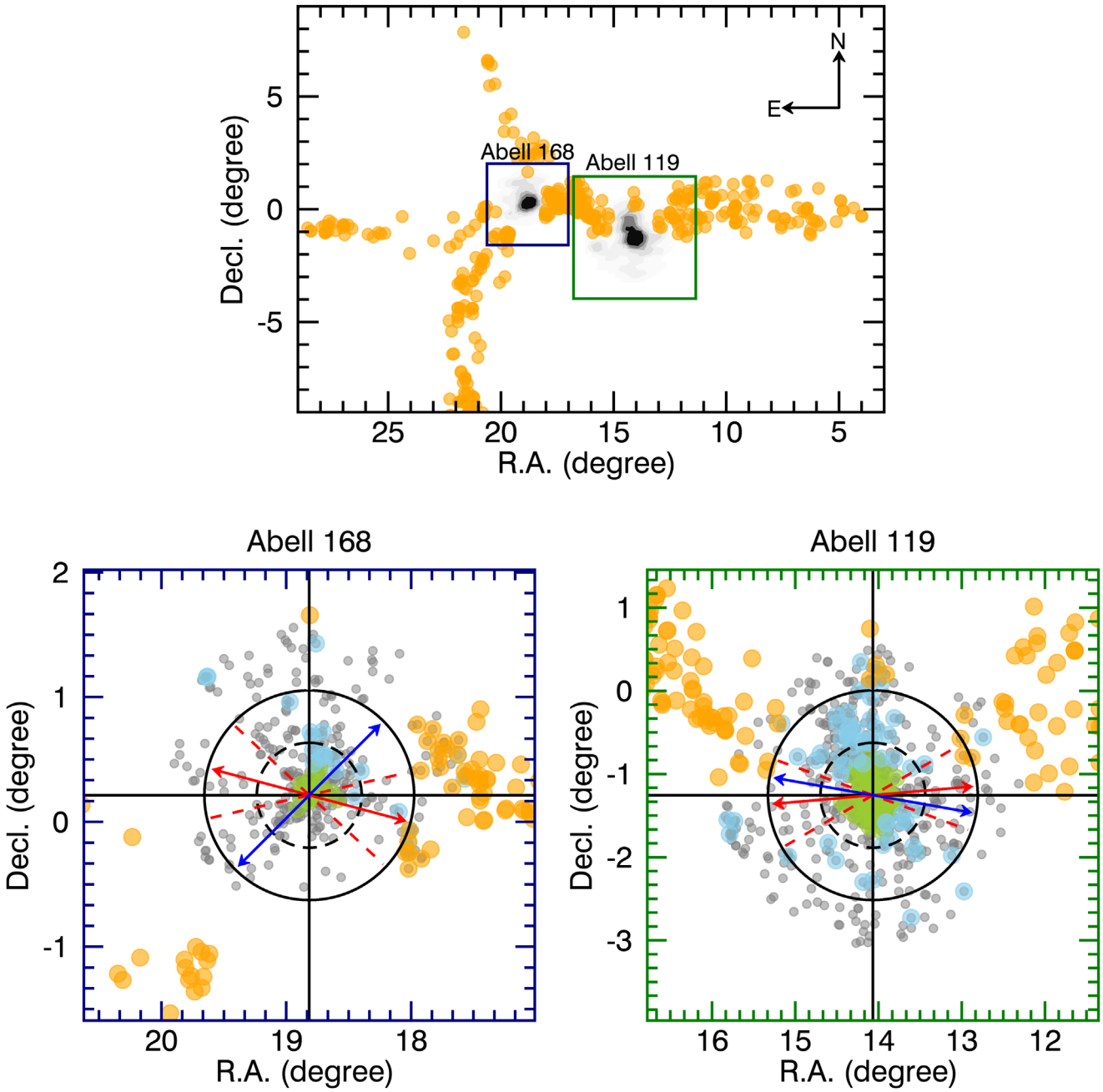

Figure 12. Top: spatial distribution of galaxies in the filaments around A119 and A168. The orange symbols show galaxies belonging to the filaments, while the contours are a number density of cluster members. Bottom: central parts of A168 (left) and A119 (right), as indicated by the blue box or the green box in the top panel, with member galaxies of each cluster (gray circles). Our luminous early-type sample galaxies are also presented as light green (ancient infallers) or sky blue (infalling populations) circles, and the red arrow denotes the kinematic position angle of each cluster. The range of the kinematic position angle is also indicated by the red dashed lines, and the additional kinematic position angle associated with infalling populations of each cluster is denoted by the blue arrow in each panel. The black dashed and solid circles indicate the R_{200} and $2R_{200}$ of each cluster.

to vary according to their surrounding filamentary structures. In this sense, to understand the kinematic alignments of cluster early-type galaxies, it is important to investigate the filamentary structures around clusters.

To identify the filamentary structures around A119 and A168, we extract all galaxies with spectroscopic information in the region of $0° < \mathrm{R.A.} < 30°$ and $-12° < \mathrm{decl.} < 16°$ from the HyperLeda database[30] and then investigate their consecutive distributions in various radial velocity ranges and mapping all selected galaxies in the three-dimensions of the Cartesian supergalactic coordinate system, following the method of Kim et al. (2016). During this process, galaxies within 2 R_{200} from the center of each cluster in supergalactic coordinates are intentionally excluded to avoid contamination from the cluster galaxies. More details about the filamentary structures around A119 and A168 will be described in a forthcoming paper (W. Lee et al. 2019, in preparation).

In Figure 12, we show the projected spatial distributions of galaxies belonging to the filaments of A119 and A168 as orange circles, with cluster members (contours in the top panel

[30] http://leda.univ-lyon1.fr/

Table 3
The Properties of Our Luminous Early-type Sample Galaxies in A119 and A168

Galaxy Name	Cluster	R.A. J2000	Decl. J2000	M_r (mag)	PA_{phot} (degree)	PA_{kin} (degree)	Ellipticity	Phase-space Class
9011900001	A119	14.06715	−1.25537	−23.48	33	155	0.23	R1
9011900006	A119	14.07562	−1.24184	−21.22	47	157	0.13	R1
9011900011	A119	14.05587	−1.23840	−19.79	135	−999	0.58	R1
9016800001	A168	18.73997	0.43081	−23.02	154	162	0.17	R1
9016800002	A168	18.73500	0.43960	−19.90	134	104	0.07	R1
9016800014	A168	18.78058	0.46580	−21.32	13	17	0.45	R2

Note. The columns give the galaxy name, cluster name, coordinate (R.A. and decl.), absolute *r*-band magnitude, photometric position angle, kinematic position angle (if SAMI IFS data is available, −999 means that the galaxy has not been observed by SAMI), ellipticity, and phase-space classification (R1 implies ancient infaller and R2 implies infalling population) for each galaxy.

(This table is available in its entirety in machine-readable form.)

and gray circles in two bottom panels). We see in the top panel that the filament connected to A119 from the west of the cluster center is wider and longer than the others. It is also noteworthy that the filamentary structure of A168 is more complex than that of A119.

The bottom-right panel shows the central part of A119, as indicated by the green box in the top panel. In the case of A119, we identify two filaments, one connected to the cluster center from the west (main filament), and the other linked to the northern part of the cluster from the northeast (northeast filament). Considering the scales and positions of the two filaments, the majority of galaxies in A119 are likely to fall into the cluster through the main filament, whereas the substructure extending to the northeast of the cluster center may be due to galaxies falling into the cluster through the northeast filament. Because the orientation of these two filaments is coincidentally similar to ∼90°, A119 appears to have only one peak in the PA distribution (see Figure 4). Moreover, the coincidence between the kinematic alignment angle of A119 (∼95°) and the directions of the main and northeast filaments suggests that the orientation of the spin axes of our sample galaxies in A119 is strongly related to the filamentary structures around this cluster.

In the bottom-left panel, we present the central part of A168, as denoted by the blue box in the top panel. As already described above, A168 is connected to at least four filaments[31] simultaneously. Such a complicated structure can lead to a random distribution of galaxy spin axes, but early-type galaxies in this cluster are kinematically aligned with each other (see Figure 9). Although the alignment signal of A168 is weaker than that of A119, considering the alignment angle of A168 of ∼75°, many early-type galaxies in A168 are likely to have flowed from the filaments located in the west and/or east directions from the cluster center. In addition, another kinematic alignment angle of ∼135° formed by infalling populations in A168 seems to be related to the filament connected to the cluster from the south.

As predicted by simulations and observational studies (see, e.g., Codis et al. 2012; Tempel et al. 2013; Dubois et al. 2014; Pahwa et al. 2016), a large number of late-type galaxies are likely to prefer PAs roughly 90° off the kinematic alignment angle of early-type galaxies. However, if the kinematic alignment angle of early-type galaxies is indeed correlated with the large-scale structures around clusters, some late-type galaxies formed by mergers in filaments are expected to show a similar PA distribution with early-type galaxies. In a forthcoming companion paper, we will explore the kinematic alignments of late-type galaxies in cluster environments.

This study has looked into the kinematic alignment of cluster early-type galaxies to understand the build-up mechanism of galaxy clusters in terms of the accretion of galaxies along filamentary structures. Using both PA_{phot} and PA_{kin}, we find that the luminous early-type galaxies in A119 and A168 are kinematically aligned with each other, and the alignment angles are closely related to the directions of the filaments around A119 and A168. This implies that cluster early-type galaxies have been accreted along filaments while maintaining their predetermined spin axes, as suggested by Kim et al. (2018) and Lee et al. (2018). Our findings provide a piece of evidence that the kinematic alignment of early-type galaxies in cluster environments can be a common phenomenon. By investigating other clusters in different dynamical status, from clusters undergoing a major cluster–cluster merger to relaxed clusters, we will know whether the cluster-to-cluster variation is mainly due to their surrounding large-scale structures or not. This gives valuable information on the formation and evolution of galaxy clusters and large-scale structures. To facilitate follow-up studies, we provide a catalog of our sample galaxies presented in this paper in Table 3.

We thank the anonymous referee for constructive comments that improved the clarity of the manuscript. H.J. acknowledges support from the Basic Science Research Program through the National Research Foundation of Korea (NRF), funded by the Ministry of Education (NRF-2013R1A6A3A04064993). M.S.O. acknowledges the funding support from the Australian Research Council through a Future Fellowship (FT140100255). J.v.d.S. is funded under Bland-Hawthorn's ARC Laureate Fellowship (FL140100278). S.K.Y. acknowledges support from the Korean National Research Foundation (2017R1A2A1A05001116) and by the Yonsei University Future Leading Research Initiative (2015-22-0064). This study was performed under the umbrella of the joint collaboration between Yonsei University Observatory and the Korean Astronomy and Space Science Institute. J.B. acknowledges support of an Australian Research Council Future Fellowship (FT180100231). S.C.R was supported by the Basic Science Research Program through the NRF of Korea funded by the

[31] It is not clear whether the southern and eastern filaments are fully connected to the cluster or not. It seems that it is due to the data completeness problem of HyperLeda, but if the disconnection is real, this might be the reason that the alignment signal of A168 is not significantly weakened despite its complex filamentary structures.

Ministry of Education (2018R1A2B2006445). Support for this work was also provided by the NRF to the Center for Galaxy Evolution Research (2017R1A5A1070354). S.B. acknowledges the funding support from the Australian Research Council through a Future Fellowship (FT140101166). N.S. acknowledges support of a University of Sydney Postdoctoral Research Fellowship. Support for AMM is provided by NASA through Hubble Fellowship grant #HST-HF2-51377 awarded by the Space Telescope Science Institute, which is operated by the Association of Universities for Research in Astronomy, Inc., for NASA, under contract NAS5-26555. J.B.H. is supported by an ARC Laureate Fellowship that funds Jesse van de Sande and an ARC Federation Fellowship that funded the SAMI prototype. Parts of this research were conducted by the Australian Research Council Centre of Excellence for All Sky Astrophysics in 3 Dimensions (ASTRO 3D), through project number CE170100013.

The SAMI Galaxy Survey is based on observations made at the Anglo-Australian Telescope. The Sydney-AAO Multi-object Integral field spectrograph (SAMI) was developed jointly by the University of Sydney and the Australian Astronomical Observatory. The SAMI input catalog is based on data taken from the Sloan Digital Sky Survey, the GAMA Survey and the VST ATLAS Survey. The SAMI Galaxy Survey is supported by the Australian Research Council Centre of Excellence for All Sky Astrophysics in 3 Dimensions (ASTRO 3D), through project number CE170100013, the Australian Research Council Centre of Excellence for All-sky Astrophysics (CAASTRO), through project number CE110001020, and other participating institutions. The SAMI Galaxy Survey website is http://sami-survey.org/.

Facilities: AAT.

ORCID iDs

Suk Kim https://orcid.org/0000-0002-3738-885X
Matt S. Owers https://orcid.org/0000-0002-2879-1663
Hak-Sub Kim https://orcid.org/0000-0001-7033-4522
Youngdae Lee https://orcid.org/0000-0002-6261-1531
Jaehyun Lee https://orcid.org/0000-0002-6810-1778
Sukyoung K. Yi https://orcid.org/0000-0002-4556-2619
Sarah Brough https://orcid.org/0000-0002-9796-1363
Anne M. Medling https://orcid.org/0000-0001-7421-2944
Sarah M. Sweet https://orcid.org/0000-0002-1576-2505
Joss Bland-Hawthorn https://orcid.org/0000-0001-7516-4016
Samuel N. Richards https://orcid.org/0000-0002-5368-0068

References

Allen, J. T., Croom, S. M., Konstantopoulos, I. S., et al. 2015, MNRAS, 446, 1567
Aragón-Calvo, M. A., van de Weygaert, R., Jones, B. J. T., & van der Hulst, J. M. 2007, ApJL, 655, L5
Aryal, B., & Saurer, W. 2004, A&A, 425, 871
Aryal, B., & Saurer, W. 2005, A&A, 432, 841
Bertin, E., & Arnouts, S. 1996, A&AS, 117, 393
Bland-Hawthorn, J., Bryant, J. J., Robertson, G., et al. 2011, OExpr, 19, 2649
Brunino, R., Trujillo, I., Pearce, F. R., & Thomas, P. A. 2007, MNRAS, 375, 184
Bryant, J. J., Bland-Hawthorn, J., Fogarty, L. M. R., Lawrence, J. S., & Croom, S. M. 2014, MNRAS, 438, 869
Bryant, J. J., Ower, M. S., Robotham, A. S. G., et al. 2015, MNRAS, 447, 2857
Caldwell, N., & Rose, J. A. 1997, AJ, 113, 492
Caldwell, N., Rose, J. A., Sharples, R. M., Ellis, R. S., & Bower, R. G. 1993, AJ, 106, 473
Cappellari, M., & Emsellem, E. 2004, PASP, 116, 138
Choi, H., & Yi, S. K. 2017, ApJ, 837, 68
Codis, S., Pichon, C., Devriendt, J., et al. 2012, MNRAS, 427, 3320
Croom, S. M., Lawrence, J. S., Bland-Hawthorn, J., et al. 2012, MNRAS, 421, 872
Driver, S. P., Hill, D. T., Kelvin, L. S., et al. 2011, MNRAS, 413, 971
Dubois, Y., Pichon, C., Welker, C., et al. 2014, MNRAS, 444, 1453
Fabricant, D., Kurtz, M., Geller, M., et al. 1993, AJ, 105, 788
Ferrari, C., Benoist, C., Maurogordato, S., Cappi, A., & Slezak, E. 2005, A&A, 430, 19
Fogarty, L. M. R., Scott, N., Owers, M. S., et al. 2014, MNRAS, 443, 485
Fogarty, L. M. R., Scott, N., Owers, M. S., et al. 2015, MNRAS, 454, 2050
Green, A. W., Croom, S. M., Scott, N., et al. 2018, MNRAS, 475, 716
Hahn, O., Teyssier, R., & Carollo, C. M. 2010, MNRAS, 405, 274
Hallman, E. J., & Markevitch, M. 2004, ApJL, 610, L81
Hoyle, F. 1949, MNRAS, 109, 365
Huchra, J. P., Macri, L. M., Masters, K. L., et al. 2012, ApJS, 199, 26
Hwang, H. S., & Lee, M. G. 2009, MNRAS, 397, 2111
Kim, S., Jeong, H., Lee, J., et al. 2018, ApJL, 860, L3
Kim, S., Rey, S.-C., & Bureau, M. 2016, ApJ, 833, 207
Kranović, D., Cappellari, M., de Zeeuw, P. T., & Copin, Y. 2006, MNRAS, 366, 787
Kranović, D., Emselem, E., Cappellari, M., et al. 2011, MNRAS, 414, 2923
Lee, J. 2004, ApJL, 614, L1
Lee, J., Kim, S., Jeong, H., et al. 2018, ApJ, 864, 69
Lee, Y., Rey, S.-C., Hilker, M., et al. 2016, ApJS, 822, 92
Navarro, J. F., Abadi, M. G., & Steinmetz, M. 2004, ApJL, 613, L41
Noble, A. G., W˙ebb, T. M. A., Muzzin, A., et al. 2013, ApJ, 768, 118
Oh, S., Yi, S. K., Cortese, L., et al. 2016, ApJ, 832, 69
Owers, M. S., Allen, J. T., Baldry, I., et al. 2017, MNRAS, 468, 1824
Pahwa, I., Libeskind, N. I., Tempel, E., et al. 2016, MNRAS, 457, 695
Paz, D. J., Stasyszyn, F., & Padilla, N. D. 2008, MNRAS, 389, 1127
Peebles, P. J. E. 1969, ApJ, 155, 393
Rhee, J., Smith, R., Choi, H., et al. 2017, ApJ, 843, 128
Rossetti, M., & Molendi, S. 2010, A&A, 510, A83
Scott, N., van de Sande, J., Croom, S. M., et al. 2018, MNRAS, 481, 2299
Sharp, R., Allen, J. T., Fogarty, L. M. R., et al. 2015, MNRAS, 446, 1551
Sharp, R., Saunders, W., Smith, G., et al. 2006, Proc. SPIE, 6269, 62690G
Tempel, E., & Libeskind, N. I. 2013, ApJL, 775, L42
Tempel, E., Stoica, R. S., & Saar, E. 2013, MNRAS, 428, 1827
Trujillo, I., Carretero, C., & Patiri, S. G. 2006, ApJL, 640, L111
van de Sande, J., Bland-Hawthorn, J., Fogarty, L. M. R., et al. 2017, ApJ, 845, 104
Wang, P., & Kang, X. 2018, MNRAS, 473, 1562
Weijmans, A. M., de Zeeuw, P. T., Emsellem, E., et al. 2014, MNRAS, 444, 3340
White, S. D. M. 1984, ApJ, 286, 38
York, D. G., Adelman, J., John, E., et al. 2000, AJ, 120, 1579